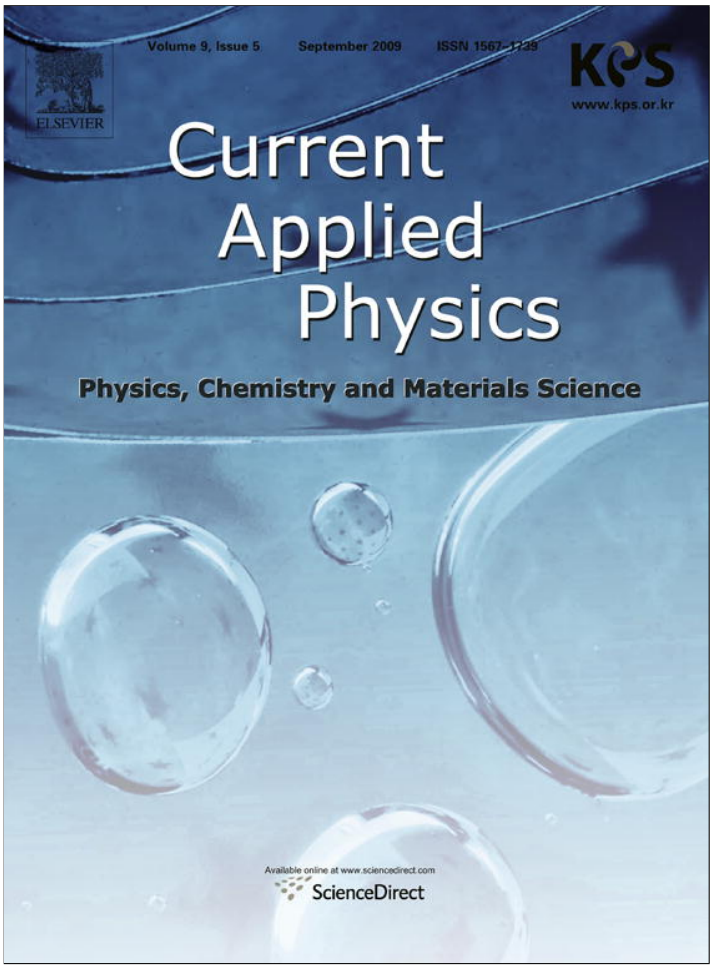

Current Applied Physics 9 (2009) 928–932

Contents lists available at ScienceDirect

Current Applied Physics

journal homepage: www.elsevier.com/locate/cap

Sintering kinetic measurement of nickel nanoparticle agglomerates by electrical mobility classification

Young Kyun Moon [a], Jae Keun Lee [b], Jin Gon Kim [a], Myung Young Jung [a], Jae Beom Lee [c], Soo H. Kim [a,*]

[a] Department of Nanosystem and Nanoprocess Engineering, Pusan National University, 50 Cheonghak-ri, Samnangjin-eup, Miryang-si, Gyeongnam 627-706, Republic of Korea
[b] School of Mechanical Engineering, Pusan National University, 30, Jangjeon-dong, Geumjeong-gu, Busan 609-735, Republic of Korea
[c] Department of Nanomedical Engineering, Pusan National University, 50 Cheonghak-ri, Samnangjin-eup, Miryang-si, Gyeongnam 627-706, Republic of Korea

ARTICLE INFO

Article history:
Received 2 June 2008
Accepted 4 June 2008
Available online 21 September 2008

PACS:
60

Keywords:
Nickel
Agglomerates
Sintering
Electrical mobility
Laser ablation

ABSTRACT

The gas-phase sintering kinetics of nickel nanoparticle agglomerates was investigated by a two step electrical mobility classification. The first electrostatic classifier sorted the agglomerated mono-area nickel nanoparticles generated by pulsed laser ablation, and then the subsequent heating process created the sintered nickel nanostructures. The second electrostatic classifier combined with the condensation nucleus counter scanned the shrinkage of the agglomerated mono-area nickel nanoparticles due to the sintering process. The change in the mono-area particle mobility size measured by the electrical mobility classification technique was compared with the results of the existing coalescence model to extract the kinetic parameters for the sintering of nickel particles. The optimum activation energy found in this study was ~63 kJ/mol, which falls between the diffusion of nickel atoms (~49 kJ/mol) and the migration and coalescence of nickel particles (~78 kJ/mol).

1. Introduction

Aerosol particle generating processes (e.g. diffusion flame, laser ablation, and condensation–evaporation methods) often produce highly agglomerated nanoparticle clusters. For the potential applications of functional nanoparticles, separated and spherical nanoparticles are preferred, because one can easily predict their behaviors and fundamental properties based on their known size and shape. Generally, when primary nanoparticles are formed in the gas phase, they begin to grow via the competition between the coagulation and sintering processes. To control the morphology of nanoparticles in the gas phase, it is necessary to disturb either the coagulation or sintering process. If the coagulation takes place much faster than the sintering process, highly agglomerated fractal-like particles can easily be obtained, which have a higher specific surface area and reactivity. However, to obtain separated particles with a single primary size, the sintering process should be enhanced so that the highly agglomerated particles are able to reshape and eventually fuse into a single primary particle.

Numerous researchers have investigated the sintering kinetics of metal and metal oxide particles with broad size distributions, which mask the effect of the size-dependent factors on the sintering behavior [1–3]. To measure the extent of restructuring of sintered particles, Shimada et al. [4] and Weber and Friedlander [5] employed a tandem differential mobility analyzer (TDMA), which enabled them to investigate the sintering kinetics of various types of particles by the electrical mobility classification technique. Shimada et al. [4] described the sintering mechanism of agglomerated silver particles based on a coalescence process, which eventually makes these agglomerated particles fuse into a single primary particles. However, Weber and Friedlander [5] proposed another sintering mechanism, in which agglomerated silver or copper particles were compacted by the rearrangement of the primary particles. Later, Karlsson et al. [6] proposed that the compacting behavior of agglomerated nanoparticles is strongly material-dependent and predominantly occurs by the self-diffusion of the metal atoms.

To date, the sintering kinetics of various metals (e.g. Au, Ag, Cu, Fe, etc.) and metal oxides (e.g. TiO_2, SiO_2, SnO_2, etc.) has been intensively studied [1–6]. However, the sintering kinetics of nickel has been rarely explored. The importance of nickel nanoparticles is highlighted by their important role as a catalytic seed to grow carbon nanotubes, which are used as the potential building blocks for micro- and nano-scale sensors, actuators, and electronic devices. It is important to obtain knowledge about the sintering kinetics of nickel nanoparticles, in order to control their final size and morphology, which can strongly affect the nanostructures (i.e. diameter or length) of carbon materials catalytically grown on the surface of nickel particles.

* Corresponding author.
E-mail address: sookim@pusan.ac.kr (S.H. Kim).

1567-1739/$ - see front matter © 2008 Elsevier B.V. All rights reserved.
doi:10.1016/j.cap.2008.06.018

In this work, the sintering process of nickel nanoparticle agglomerates is experimentally investigated by using a tandem differential mobility analyzer (TDMA). The coalescence model suggested by Seto et al. [3] is then employed to predict the change in the particle size due to their sintering behavior so that we can extract the sintering kinetics of nickel nanoparticles in the gas phase by comparing it with the experimental TDMA measurements.

2. Theoretical model

To theoretically describe the sintering process, the sectional model suggested by Seto et al. [3] was employed in this study. Briefly, the sectional model is described by the mechanism underlying the change in the surface area of agglomerated particles. The reduction rate of the surface area of sintering agglomerated particles is given by Koch and Friendlander [7],

$$\frac{da_s}{dt} = -\frac{1}{\tau}(a_s - a_{sc}), \tag{1}$$

where a_s is the surface area of the agglomerated particles at time, t, and a_{sc} is the surface area of the final single sphere after the completion of the sintering process.

In the sectional model-based calculation, the heating zone in the sintering furnace is divided into ith sections. Eq. (1) is able to be converted into an integrated form as follows,

$$a_{si} = a_{si-1}\exp\left(-\frac{\Delta t_i}{\tau_i}\right) + a_{sc}\left[1 - \exp\left(-\frac{\Delta t_i}{\tau_i}\right)\right], \tag{2}$$

where a_{si} and a_{si-1} are the surface areas of the agglomerates in the ith and $(i-1)$th sections, and τ_i is the sintering time [i.e. $\tau_i = A d_{pi}^m \exp(E/R_g T)$, where m is assumed to be 4 for grain boundary diffusion, A and E are the diffusion coefficient and activation energy, respectively, R_g is the universal gas constant, d_{pi} is the primary particle size in the ith section (i.e. $d_{pi} = 6\,V/a_{si}$), where V is the volume of the agglomerate (i.e. $V = \pi d_{pi}^3 N/6$), where N is the number of primary particles in an agglomerated cluster (i.e. $N = (d_f/d_{pi})^3$), where d_f is the final mobility size of the fully sintered nickel particle]. Also, Δt_i is the heating period in the ith section.

The calculation of Eq. (2) is repeated by increasing i by 1 until the final section is reached, viz. the ~1000th in this study. The final equivalent surface area particle diameter, d_s (i.e. $d_s = (a_s/\pi)^{1/2}$), was compared with the measured electrical mobility diameter, d_m, to extract the kinetic energy corresponding to the sintering of nickel nanoparticles in the gas phase.

3. Experimental

Fig. 1 shows a schematic of the experimental system, which consists of a pulsed laser ablation (PLA) particle source and a tandem differential mobility analyzer (TDMA) system. The PLA system consists of a 1064 nm Q-switched Nd:YAG laser beam focused with a 20 cm focal length lens onto a solid nickel target. The intense laser-induced micro-plasma at the nickel surface generates nickel vapor which is continuously swept and quenched by a 1 lpm flow of nitrogen carrier gas, so that nickel nanoparticles are formed by nucleation and coagulation. The addition of a 50 $cm^3\ min^{-1}$ (SCCM) flow of hydrogen, along with the nitrogen carrier gas, was used to suppress the possible formation of an oxide layer on the nickel particles. The nickel target was mounted on a rotating shaft with a stepper motor, so that the target could be rotated with a controlled interval to provide the particle generation process with long-term stability.

The polydisperse nickel aerosol particles generated in the PLA were then rapidly transported into DMA-1, which is incorporated within the laser ablation chamber. Since a reasonably high fraction of the PLA-generated nickel particles are singly charged due to the laser-induced plasma, the DMA was operated without any auxiliary charger. The DMA was employed as a particle size selection tool and operates on the basis of gas-phase electrophoresis, by selecting particles based on their equivalent electrical mobility. The details of the DMA are described elsewhere [8]. Briefly, the DMA typically consists of a high voltage-connected cylindrical central rod, which is aligned coaxially with an electrical ground-connected cylindrical housing. Clean dry sheath nitrogen (~10 lpm) was supplied around the central electrode, and the annular flow of PLA-generated aerosol particles (~1 lpm) was introduced from the top of the DMA column. While the majority of the metal aero-

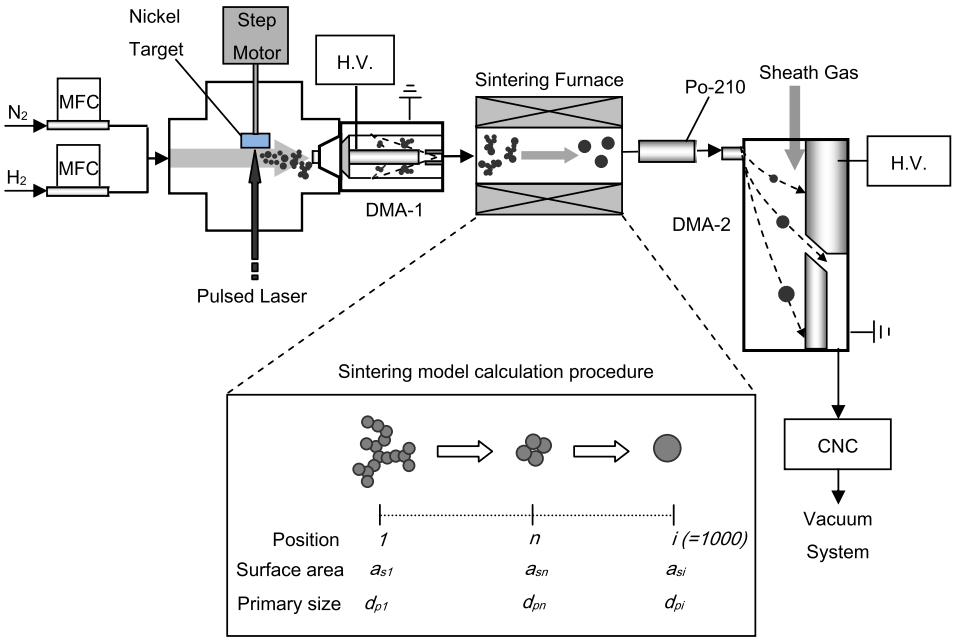

Fig. 1. Schematic of sintering model and experimental setup consisting of pulsed laser ablation and tandem differential mobility analyzer system (DMA: differential mobility analyzer, CNC: condensation nucleus counter, MFC: mass flow controller, H.V.: high voltage power supply).

sols were exhausted through the bottom of the DMA column, a fraction of the metal aerosols with equivalent electrical mobility are classified on the basis of the balance between the electrostatic attraction and drag forces, and can be extracted from the instrument. In this study, two DMAs (i.e. TDMA) were employed. DMA-1's function is to classify the singly charged mono-area particles by their electrical mobility [9]. The mono-area metal nanoparticles selected by DMA-1 were subsequently sintered in the first tube furnace (hereafter referred to as the sintering furnace) at various temperatures to form larger unagglomerated primary particles. The sintering furnace had a 2.54 cm diameter × 50 cm heating length so that the residence time was ~3 sec at ~1200 °C for a fixed 1 lpm aerosol flow rate. As a final step, DMA-2 combined with the condensation nucleus counter (CNC) scans the evolution of the resulting size distribution after sintering, to obtain the extent of shrinkage.

4. Results and discussion

The nickel nanoparticles generated by PLA in this approach have a broad particle size distribution (PSD) (i.e. standard deviation of ~1.41) with a peak relative count at a mobility size of ~60 nm, as shown in Fig. 2a. To track the temperature-dependent sintering behavior of the nickel nanoparticles, we employed two consecutive electrical mobility classification steps. First, the polydisperse nickel nanoparticles generated by PLA pass through DMA-1, and then a group of agglomerated mono-area nickel nanoparticles with the same electrical mobility and a very narrow particle size distribution (i.e. standard deviation of ~1.17) are selected, as shown in Fig. 2a. In this study, after the three initial groups of agglomerated nickel nanoparticles with sizes of 20, 32, and 52 nm, respectively, were classified by DMA-1, they were subsequently sintered at various temperatures in the sintering furnace with a residence time of ~3 sec. Then, DMA-2 was employed as a scanning tool to detect the decrease in the surface area of the sintering nickel particles, in order to directly track their sintering kinetics. Fig. 2b presents the evolution of the size distribution of the initial 52 nm size-selected nickel particles as a function of the sintering temperature. The sintering-induced shrinkage in the particle size began at ~100 °C, accelerated at medium temperatures of between 200 and 1100 °C, and stopped at temperatures higher than ~1200 °C. The initial 52 nm nickel nanoparticles were observed to be fully sintered and turned into isolated primary particles with an average size of ~20 nm. The decrease in the relative count of the number concentration of nickel particles with increasing sintering temperature is attributed to the thermophoretic deposition loss of the in-flight nickel particles to the sintering reactor wall.

To corroborate the series of TDMA measurements, TEM analysis was performed for the nickel particles sintered at various temperatures. The PLA-generated nickel nanoparticles corresponding to

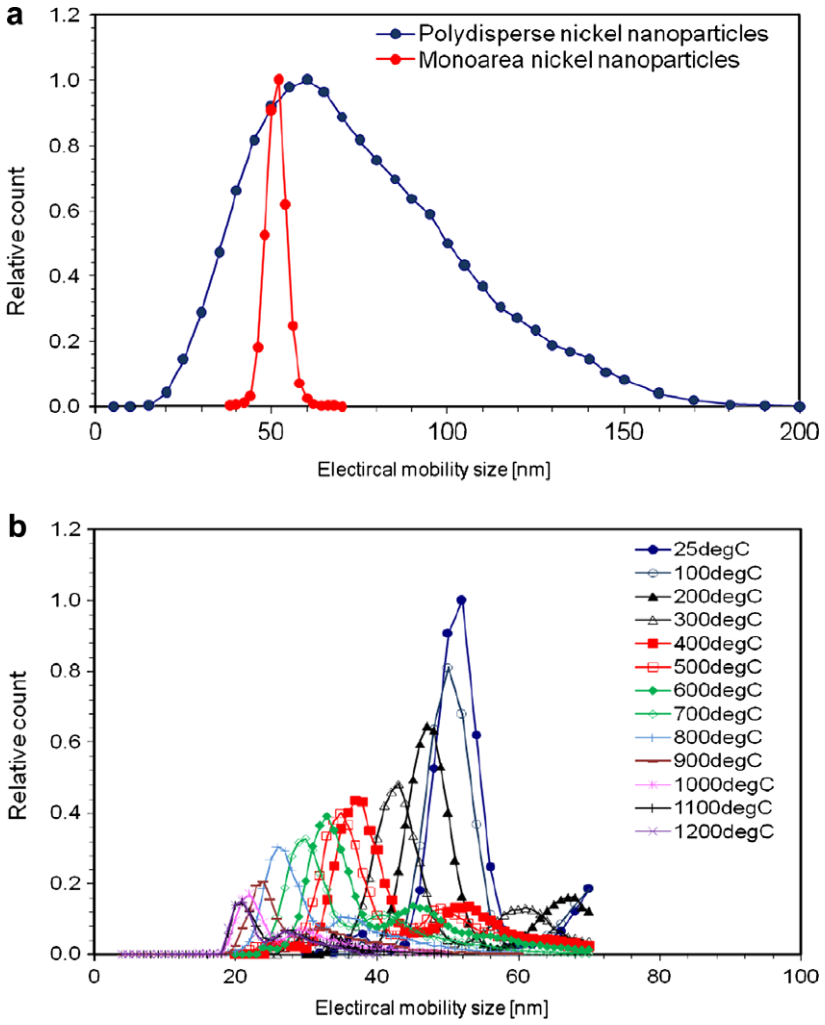

Fig. 2. (a) Mobility size distribution of polydisperse (i.e. without using DMA-1) and DMA-1 selected mono-area nickel particles measured by DMA-2 combined with a CNC, and (b) the evolution of the mobility size distribution of the initial 52 nm nickel particles at various sintering temperatures.

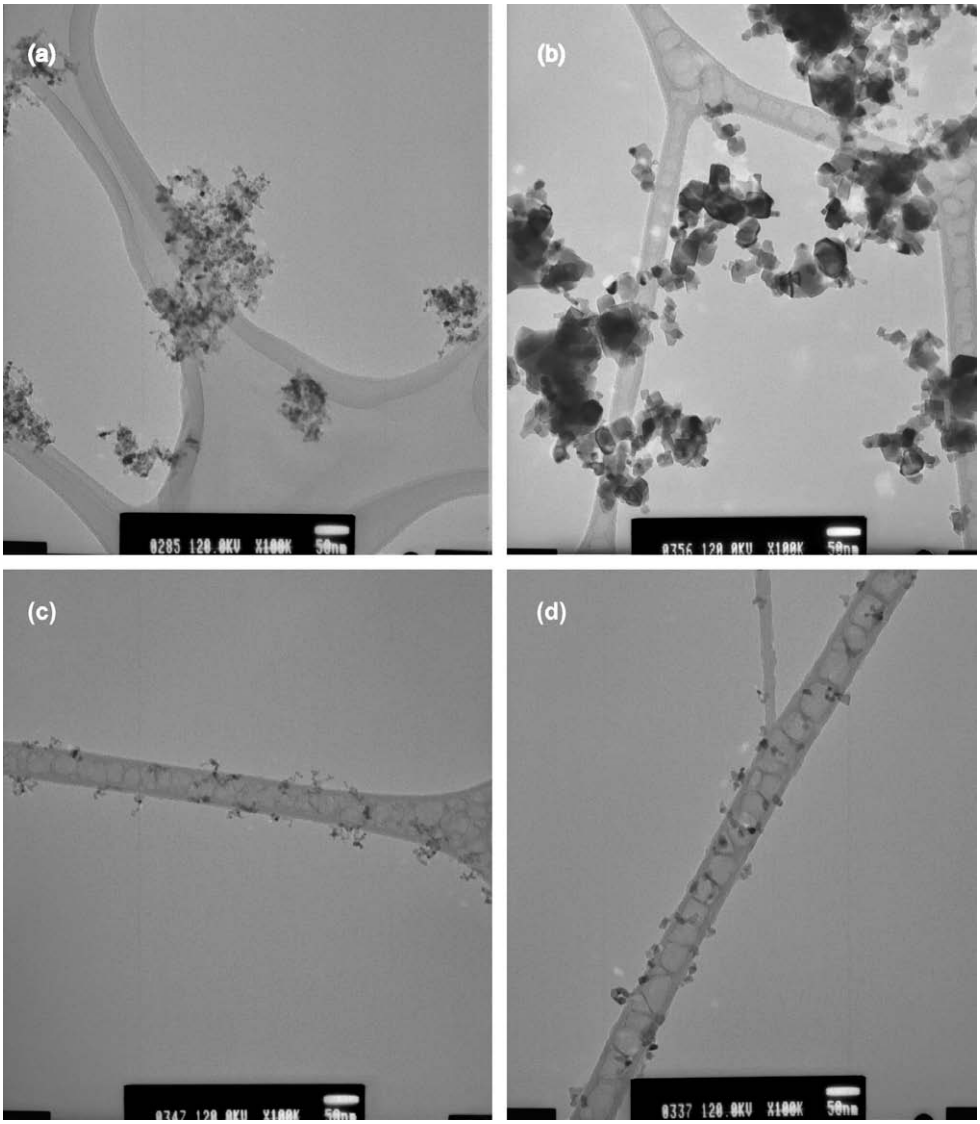

Fig. 3. (i) TEM images of PLA-generated polydisperse nickel particles (a) before and (b) after sintering process at ~1200 °C, and (ii) DMA-1 classified 32 nm mobility size mono-area nickel nanoparticles (c) before and (d) after sintering process at ~1200 °C.

the broad PSD shown in Fig. 2a were observed to be highly agglomerated with a primary size of ~5 nm, as shown in Fig. 3a. After the sintering process at ~1200 °C, the morphological change of the polydisperse nickel particles is shown in Fig. 3b, where the size of the primary particles (i.e. ~30 nm) became much bigger due to the enhanced sintering process at high temperatures. To observe the effect of sintering on the mono-area nickel particles, the polydisperse nickel agglomerated particles were first classified by DMA-1, in which randomly rotating nickel agglomerated particles in the electric field were selected by the balance between the electrostatic attraction force and drag force [9]. With the assistance of DMA-1, the agglomerated mono-area nickel nanoparticles with electrical mobility sizes of 20, 32, and 52 nm were sampled and then subsequently in-situ sintered at various temperatures in the sintering tube furnace. Fig. 3c and d show the mono-area nickel particles with an initial mobility size of 32 nm before and after sintering at ~1200 °C, respectively. After the sintering process of the DMA-1 selected mono-area particles, one can clearly see that fully sintered and isolated spherical-like nickel nanoparticles were formed, as shown in Fig. 3d, implying that the compaction of the agglomerated nickel particles is finished at temperatures higher than ~1200 °C.

On the basis of the series of TDMA measurements, the change in the experimentally measured particle size (symbols) due to the sintering behavior was compared with the theoretically predicted size (solid lines) (i.e. Eq. (2)) of the nickel particles as a function of the sintering temperature, as shown in Fig. 4. It can be seen that the continuous shrinkage in the particle mobility diameter occurred with increasing sintering temperature. However, the particle mobility diameters remained constant at certain critical temperatures, indicating that no more compaction occurred. At this point, the internal restructuring process, leading to the formation of crystallite structures, takes place. To extract the sintering kinetics of the nickel nanoparticles, we varied both the pre-exponential factor and activation energy in the coalescence model presented in Eq. (2). The best fit between the experimentally- and theoretically-determined nickel particle sizes at various temperatures and initial particle sizes was then found, as shown in Fig. 4. The optimum values of the pre-exponential factor (A) and activation energy (E_a) for the sintering nickel aerosol particles were found to be $A = \sim 1.1 \times 10^{29}$ s/m^4 and $E_a = \sim 63$ kJ/mol, respectively. Our measured activation energy (~63 kJ/mol) for the sintering of agglomerated nickel particles falls between the values for the diffusion of nickel atoms (~49 kJ/mol) [1] and the migra-

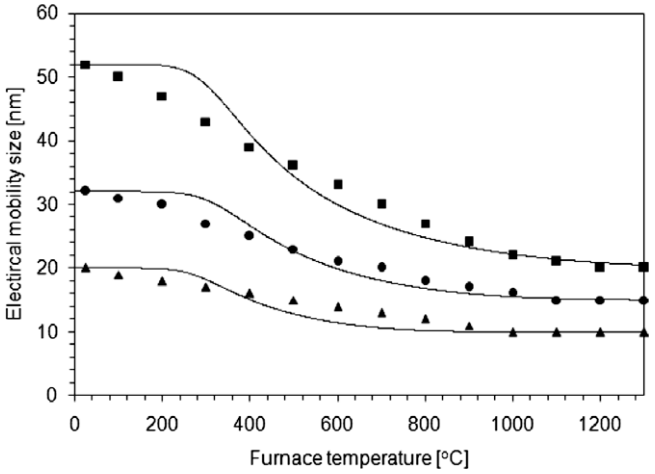

Fig. 4. Comparison of experimentally-determined particle size (symbols, TDMA measurements) with theoretically-determined particle size (solid lines, Eq. (2)) of nickel agglomerates with different initial mobility sizes of 20, 32, and 52 nm as a function of sintering temperature. The sintering kinetics parameters found were $A = \sim 1.1 \times 10^{29}$ s/m^4 and $E_a = \sim 63$ kJ/mol.

tion and coalescence of nickel particles (~78 kJ/mol) [2], implying that the gas-phase sintering of nickel nanoparticles occurred by a combination of the nickel atom migration and particle migration (i.e. coalescence) mechanisms in the temperature range of 25–1300 °C.

5. Conclusion

We investigated the sintering kinetics of agglomerated nickel aerosol nanoparticles using the TDMA technique. With the assistance of two sequential electrical mobility classification techniques, the change in the mobility size of agglomerated mono-area nickel particles was scanned, and then the sintering kinetic parameters were extracted by comparing the TDMA-measured data with the theoretical coalescence model. On the basis of the activation energy for the sintering of nickel nanoparticles found in this study, the combination of nickel atom migration and nickel particle migration (i.e. coalescence) was suggested as the sintering mechanism for agglomerated nickel aerosol nanoparticles in our approach. This sintering kinetics study also enables the shape and size of agglomerated nickel nanoparticles to be controlled by perturbing both the coagulation and sintering processes, thus providing one of potential means to process nanostructured materials.

Acknowledgement

This work was supported by the Korea Science and Engineering Foundation (KOSEF) grant funded by the Korea government (MEST) (No. R01-2008-000-10181-0).

References

[1] J. Sehested, Sintering of nickel steam-reforming catalysts, J. Catal. 217 (2003) 417.
[2] J. Sehested, J.A.P. Gelten, I.N. Remediakis, H. Bengaard, J.K. Norskov, Sintering of nickel steam-reforming catalysts: effects of temperature and steam and hydrogen pressure, J. Catal. 223 (2004) 432.
[3] T. Seto, A. Hirota, T. Fujimoto, M. Shimada, K. Okuyama, Sintering of polydisperse nanometer-sized agglomerates, Aerosol Sci. Technol. 27 (1997) 422.
[4] M. Shimada, T. Seto, K. Okuyama, Size change of very fine silver agglomerates by sintering in a heated flow, J. Chem. Eng. Japan 27 (1994) 795.
[5] A.P. Weber, S.K. Friedlander, In situ determination of the activation energy for restructuring of nanometer aerosol agglomerates, J. Aerosol Sci. 28 (2) (1997) 179.
[6] M.N.A. Karlsson, K. Deppert, L.S. Karlsson, M.H. Magnusson, J.O. Malm, N.S. Srinivasan, Compaction of agglomerates of aerosol nanoparticles: A compilation of experimental data, J. Nanoparticle Res. 7 (2005) 43.
[7] W. Koch, S.K. Friedlander, The effect of particle coalescence on the surface area of a coagulating aerosol, J. Colloid and Interface Sci. 140 (1990) 419.
[8] E.O. Knutson, K.T. Whitby, Aerosol classification by electric mobility: Apparatus, theory and applications, J. Aerosol Sci. 6 (1975) 443.
[9] S.N. Rogak, R.C. Flagan, H.V. Nguyen, The mobility and structure of aerosol, Agglomerates, Aerosol Sci. Technol. 18 (1993) 25.